



# Experimental Study on Long-Term Strength and Creep Characteristics of Sandstone Under Different Water Content and Confining Pressure

Chengyu Miao<sup>1,2</sup> · Ming Jiang<sup>1,2</sup> · Lei Wang<sup>1,2</sup> · Jinkun Yang<sup>1,2</sup> · Xiaoming Sun<sup>1,2</sup>

Received: 4 November 2023 / Accepted: 5 May 2024

© The Author(s), under exclusive licence to Springer-Verlag GmbH Austria, part of Springer Nature 2024

## Abstract

Water plays a crucial role in underground engineering, significantly influencing the short-term and long-term strength and deformation behavior of rocks. Understanding the mechanics of rock deformation under water–rock coupling is vital for assessing the stability of underground structures. In this study, short-term strength compression and creep experiments were conducted on sandstone samples with varying water contents. Critical water contents (0%, 0.8%, 1.6%, 2.4%, and 3.3%) were determined through water absorption experiments, with corresponding tests performed under confining pressures of 0 MPa, 6 MPa, 9 MPa, and 12 MPa. Results revealed an exponential decrease in uniaxial compressive strength and elastic modulus with increasing water content, while confining pressure influenced radial deformation, leading to a linear increase in compressive strength. Water content also significantly impacted micro-cohesion and internal friction angle, with cohesion being more sensitive to water. The creep experiment demonstrated a deformation trend similar to compressive strength, with analysis revealing three stages of creep deformation: viscoelastic, plastic, and nonlinear acceleration. Critical strengths entering different stages were identified, with their ratio to compressive strength stabilizing between 0.44–0.59 and 0.59–0.74. A strain parameter  $\epsilon_{ac}$ , related to steady-state and accelerated creep failure time, showed little correlation with water content but exhibited a linear relationship with confining pressure. Short-term and long-term failure modes of sandstone were analyzed, indicating a transition from “X-shaped” conjugate shear failure to single oblique shear failure with changing confining pressure and water content. Mitigation measures, such as groundwater isolation and the application of high confining pressure, were identified as effective means to mitigate long-term rock deformation's adverse effects on structural integrity in onsite engineering projects, ensuring structural stability throughout construction. The study's findings and data are crucial for informing the long-term stability of engineering structures.

## Highlights

1. Water content significantly affects the short-term and long-term strength and deformation behavior of rocks.
2. The creep behavior of rocks is influenced by water content, confining pressure, and shear stress.
3. The water content and confining pressure affect the formation and evolution of cracks in rocks during creep.
4. Different failure modes are observed in rocks, depending on water content and confining pressure.

**Keywords** Sandstone · Water–rock coupling · Water content · Confining pressure · Steady-state creep · Accelerated creep

---

✉ Xiaoming Sun  
sunxiaoming@cumtb.edu.cn

<sup>1</sup> State Key Laboratory for Tunnel Engineering, China  
University of Mining and Technology-Beijing,  
Beijing 100083, China

<sup>2</sup> School of Mechanics and Civil Engineering, China  
University of Mining and Technology-Beijing,  
Beijing 100083, China

## 1 Introduction

Mineral resource exploitation has been increasing in depth due to the growth of resource and engineering demands (He and Wang 2023; Kang et al. 2023), resulting in complex geological conditions surrounding rocks. Rock creep refers to the process of gradual growth and development of rock deformation under sustained stress, which affects the long-term stability of rock engineering, and creep destabilization damage is increasingly evident in the current process of deep-buried tunnels and deep resource extraction (Li and Xia 2000; Fabre and Pellet 2006; Damjanac and Fairhurst 2010; Tran et al. 2021; Sun et al. 2023a). Meanwhile, in the process of construction and utilization, rock engineering often encounters aquifers, leading to continuous water erosion of the ore column, making the rock prone to softening and deformation, resulting in instability damage. The softening of rocks by water not only weakens their short-term strength but also adversely affects their long-term strength (Vasarhelyi and Ván, 2006; Nara et al. 2017; Zhang et al. 2023).

Numerous domestic and international scholars have extensively researched the short-term strength of different rock types. By studying the compressive strength, elastic modulus, tensile strength, and other parameters of rocks under varying water contents, it has been discovered that the strength of rocks mainly decreases when the saturation is less than 20%. The strength decrease is not significant at higher saturation levels (Vergara and Triantafyllidis 2016; Roy et al. 2017; Zhou et al. 2018; Zhu et al. 2021; Sun et al. 2023c). The uniaxial compressive strength, elastic modulus, and tensile strength of rocks decrease by 60–90% from the dry state to the saturated state. The peak strength and residual strength increase with increasing confining pressure, and the degree to which water content affects the various parameters of rocks decreases with increasing confining pressure (Gao et al. 2015; Wu et al. 2018; Li et al. 2020; Fu et al. 2021; Chen et al. 2023). Mineral composition and porosity (Li et al. 2011; Wasantha and Ranjith 2014; Zhou et al. 2021) can also affect rock softening. Sun et al. (2023a, b, c, d) investigated the variation of clay mineral composition and the effect of clay mineral content on short-term strength under the influence of different water contents.

Numerous experimental studies on the creep mechanical properties of different rocks have been conducted by scholars at home and abroad to explore the long-term strength of rocks (Yang and Jiang 2010; Huang et al. 2021; Yang et al. 2022; Zhang et al. 2022). They analyzed the relationship between the creep properties of soft rocks, including strength, elastic modulus, creep rate, and stress and time. Some scholars have also studied the effects of temperature, pore pressure, and freeze–thaw on the creep mechanical

properties of rocks (Ngwenya et al. 2001; Heap et al. 2009; Yang et al. 2014; Chen et al. 2018; Yang and Jiang 2022; Yu et al. 2023). Sandstone has good homogeneity and structural stability, which is why numerous rock projects have been chosen in sandstone formations (Su et al. 2021; Tang et al. 2023). For the study of time-dependent deformation in sandstone, Tian et al. (2015) performed the time-dependent behavior of argillaceous red sandstone under high in situ stress and observed nonlinear changes in creep strain and volume expansion. Zhao et al. (2021) studied the rock creep AE model and the characteristics of AE during the accelerating creep stage. Pan and Zhou (2022) studied the creep damage mechanism of sandstone by combining the change characteristics of porosity and the characteristics of creep deformation of sandstone sample during the creep stage. Additionally, scholars have conducted water–rock coupling creep experiments on various rocks to study the influence of water–rock coupling on long-term strength (Yu et al. 2019; Yan et al. 2020; Lin et al. 2022). The experiments found that saturated samples enter the creep deformation stage at lower stress levels, and the cumulative creep deformation of saturated samples is much greater than that of dry samples (Liu et al. 2021; Li et al. 2022; Tang et al. 2022). The elastic modulus and uniaxial compressive strength significantly decrease with increasing water content, and the creep deformation and steady-state creep rate increase with increasing water content (Tang et al. 2018; Mei et al. 2021). Considering the deteriorating effect of water content on rock strength, Deng et al. (2016) studied the effect of water–rock cycle times on the creep deformation law of sandstone and found that the creep damage stress and long-term strength decreased by 55% and 60%, respectively, after the first three water–rock cycles. Sun et al. (2021) and Sun et al. (2023b) conducted uniaxial compression creep experiments on sandstone under different water contents and found that the creep damage stress and long-term strength of sandstone decrease exponentially with increasing water content, and the attenuation creep stage time decreases with increasing water content and increases with increasing stress level. Lin et al. (2022) conducted triaxial compression creep experiments on sandstone under different water contents (confining pressure of 20 MPa), and found that the instantaneous strain, creep strain, and steady-state creep strain rate significantly increased with increasing water content and stress level, shortening the shear dilation time and failure time. Li et al. (2022) conducted graded unloading triaxial creep tests on shale with different water contents and found that the creep deformation of shale is affected by both confining pressure and saturation coefficient. Tang et al. (2018), Yu et al. (2019), Chen et al. (2021), and Tang et al. (2022) studied the effect of immersion conditions on the creep deformation law of rock sample sand found that the creep deformation of rocks is affected by the immersion temperature,

immersion time, and water content. The creep deformation rate increases with increasing immersion temperature, immersion time, and water content. The creep deformation of rocks is also affected by the mineral composition, porosity, and microstructure of the rock samples (Yang et al., 2021; Zhou et al., 2022). The vast majority of previous experiments were conducted under specific water content conditions, such as dry, natural, saturated, and single pressure states. These studies do not provide a comprehensive understanding of the entire rock creep process under varying water content and confining pressure conditions. Furthermore, the investigation into the coupling effect between pressure at different depths and creep stress within the study of creep laws remains an area requiring further investigation.

In summary, the long-term strength of rocks is influenced by a variety of factors, including water content, confining pressure, mineral composition, porosity, and time. Understanding the creep properties of rocks is crucial for the design, construction, and maintenance of rock engineering. Therefore, this paper combines the practical problems of the Wanfu coal mine project, takes the -950 level pump house access sandstone as the research object, conducts graded loading creep experiments according to the key water content state established by water absorption experiments, and simultaneously considers the three-dimensional stress state of the surrounding rock at different depths to carry out creep experiments, to deeply study the creep and deformation law of sandstone under the hydrodynamic coupling effect. The research results have enriched the field of rock creep mechanics and enhanced the understanding of sandstone creep mechanical properties under hydraulic coupling.

## 2 Creep Experiment Preparation

### 2.1 Engineering Background

The Wanfu Coal Mine, situated in the southern part of Juye Coalfield in Heze City, Shandong Province, China, possesses the thickest alluvial layer cover among all mines in the country. The mine is divided into two levels: the -820 level and the -950 level. The horizontal pump room at a depth of approximately 1040 m is affected by direct water-filling aquifers in the roof and floor. Between November 2016 and February 2019, the mine had a monthly average water inflow of up to 485.7 m<sup>3</sup>/h (in August 2017), with an average of 219.09 m<sup>3</sup>/h. The mine's high groundwater influence, high burial depth, and high stress levels have resulted in varying degrees of damage to the chambers. Combined with the dense layout of the chambers and the high level of construction disturbances,

this has posed a significant challenge to the construction of the mine. Therefore, studying the creep mechanical properties of rocks under different water content and different confining pressure states is of great significance for the safe and efficient mining of Wanfu coal mine.

### 2.2 Sample Preparation

On-site drilling of rock cores and processing them into cylindrical samples ( $\Phi 50 \times 100$  mm) were performed according to the recommended standards of the International Society of Rock Mechanics (ISRM) (Hawkins et al. 2009), which ensured that the surface flatness and parallelism of the upper and lower ends were within the specified error range. The average wave speed was 3.52 km/s, and samples with similar wave speeds were selected for the experiments. X-Ray Diffraction (XRD) and Scanning Electron Microscopy (SEM) experiments (Miao et al. 2021) revealed that the sandstone samples were primarily composed of quartz particles as the primary framework, with kaolinite as the primary clay mineral filling in the intergranular pores and particle cracks (Fig. 1). The samples were dried at a constant temperature of 105 °C until reaching a constant quality, which took about 24 h, to ensure that they were in a dry state. The sandstone samples had an average natural water content of 0.3% under laboratory conditions, while the natural dry water content of field samples ranged from 0.62 to 1.78%. The average dry density of the samples was 2403 g/m<sup>3</sup>.

### 2.3 Water Absorption Experiment

Before conducting compression experiments, non-pressure water absorption tests (Wong and Jong 2014) were performed on three sandstone samples using the laboratory deep soft rock hydraulic testing system (Fig. 2). The dry rock samples were placed on the water absorption base and submerged 3 mm into deionized water, with stable temperature and humidity ensured. During the experiment, the water absorption data acquisition system was activated, and the experiment ended when the sandstone sample reached saturation, achieving adsorption and evaporation equilibrium with the surrounding environment. The water content at different stages of water absorption was recorded, and Eq. (1) was used to calculate the water content

$$W = (M_w - M_0) / M_0 \times 100\% \quad (1)$$

where  $t$  represents time,  $w$  represents the sandstone water content at time  $t$ ,  $M_w$  represents the amount of water absorbed by the sandstone at time  $t$ , and  $M_0$  represents the mass of the sandstone sample in a dry state.

As shown in Fig. 3, the water absorption of the sample increased sharply in the first 31 h, and then entered a stable

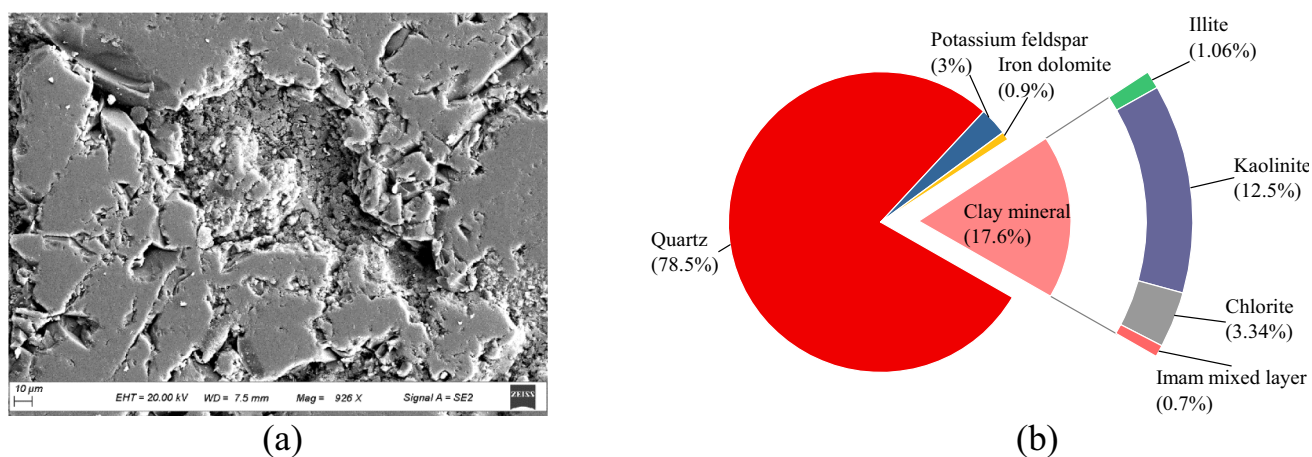


**Fig. 1** Sandstone microstructure monitoring experiment: **a** scanning electron microscope (SEM) image of the sandstone used in this study; **b** pie chart showing the mineral composition of the studied sandstone

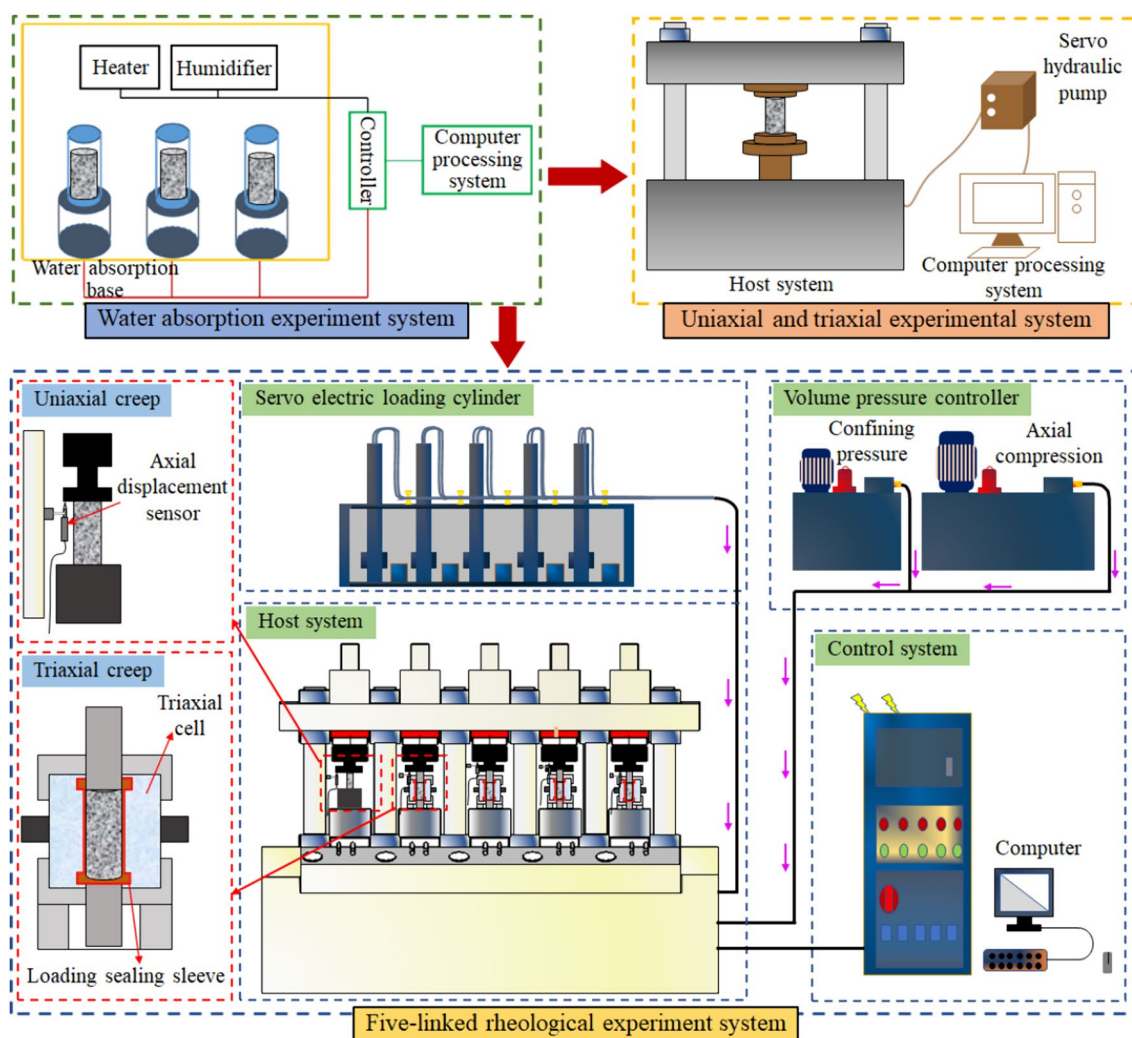


**Fig. 2** Simulation diagram of experimental system

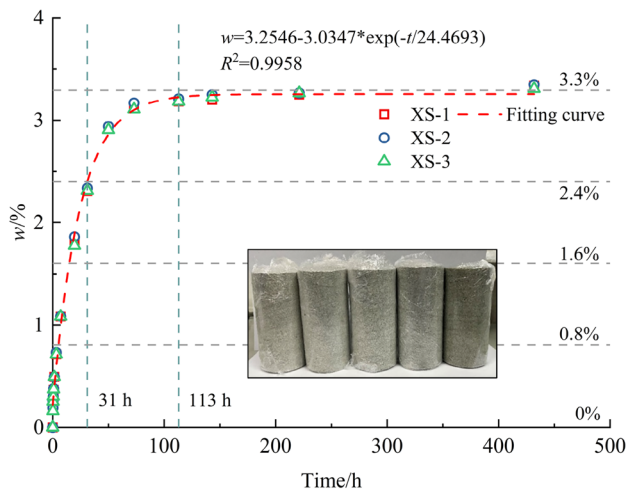


Fig.3 Water absorption curves for the water content of the sandstone

and slow water absorption stage after 113 h. The quality of the sample hardly changed when it was carried out for 432 h. It was considered that the sample had reached the limit saturation state (water content of 3.43%). To obtain a continuous and accurate softening law of sandstone strength with respect to water content, we designed five different water content levels for water absorption softening tests: 0%, 0.8%, 1.6%, 2.4%, and 3.3%. Figure 3 shows some of the experimental samples. To prevent changes in the water content of the rock samples during transportation, we wrapped the samples in PE film to reduce moisture loss. The water content of the samples was measured again before conducting the mechanical experiments to obtain an accurate water content status. A negative exponential function was used to fit the relationship between water content and time, as shown in Fig. 3.

### 2.4 Short-Term Strength Experiment

Sandstone samples with different water contents were subjected to short-term compressive strength experiments using a 2000 kN rock single-triaxial experimental system (Fig. 2). Based on hydraulic fracturing ground stress test data from Wanfu Coal Mine, the minimum principal stresses typically range from 10.4 to 20.8 MPa. This study aims to examine the creep mechanical properties of rock samples, with a focus on achieving greater accuracy under lower surrounding pressure conditions. Hence, pressure levels of 0 MPa, 6 MPa, 9 MPa, and 12 MPa were selected to mimic sandstone behavior at various geological depths or under diverse ground stress conditions. The experiments investigated the effect of different water contents on the short-term strength of rocks and determined the creep stress at the corresponding water content state. The samples were loaded until failure using a

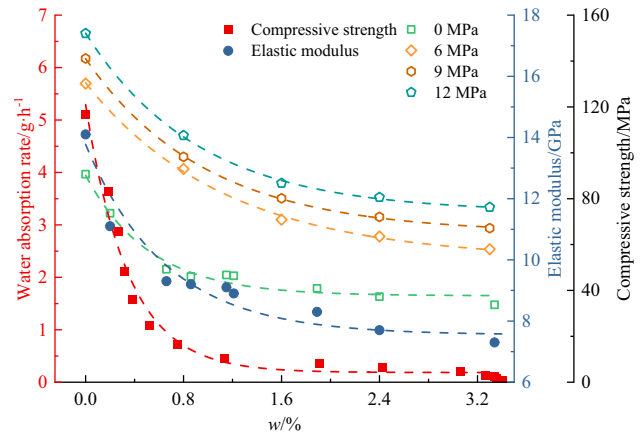


Fig. 4 Water softening curve of water absorption rate and compressive strength

constant loading rate of 0.05 kN/s, and stress and displacement data were recorded.

Figure 4 shows the water softening curve of water absorption rate and compressive strength ( $\sigma_c$ ), which indicates that water has a significant impact on the mechanical properties of rocks. As the water content increases, the uniaxial compressive strength and modulus of elasticity ( $E$ ) decreased from initial values of 90.67 MPa and 14.1 GPa to 33.74 MPa and 7.3 GPa. Uniaxial compression experiments were conducted on sandstone samples saturated for 15 days. The average uniaxial compressive strength was 31.82 MPa, and the elastic modulus was 7.33 GPa, with little difference in strength. Furthermore, the triaxial compressive strength was observed to increase with increasing confining pressure and decrease nonlinearly with increasing water content. When the confining pressure was 12 MPa, the compressive strength decreased from 152.02 MPa to 76.29 MPa as the water content increased from dry to saturation.

According to the Mohr–Coulomb strength theory, the internal friction angle and cohesion of rock can be calculated based on the relationship between the maximum and minimum principal stresses, as shown in Eq. (2)

$$\sigma_1 = \sigma_3 \tan^2 \left( 45^\circ + \frac{\varphi}{2} \right) + 2c \tan \left( 45^\circ + \frac{\varphi}{2} \right) \quad (2)$$

where  $\sigma_1$  represents maximum principal stresses (axial stress),  $\sigma_3$  represents minimum principal stresses (confining pressure),  $\varphi$  represents internal friction, and  $c$  represents cohesion.

The cohesion and angle of internal friction decreased from 18.93 MPa and 45.96° in the dry state to 8.14 MPa and 39.75° in the saturated state. With the increase in water content, both cohesion and angle of internal friction show a negative exponential decrease trend, and the effect of water

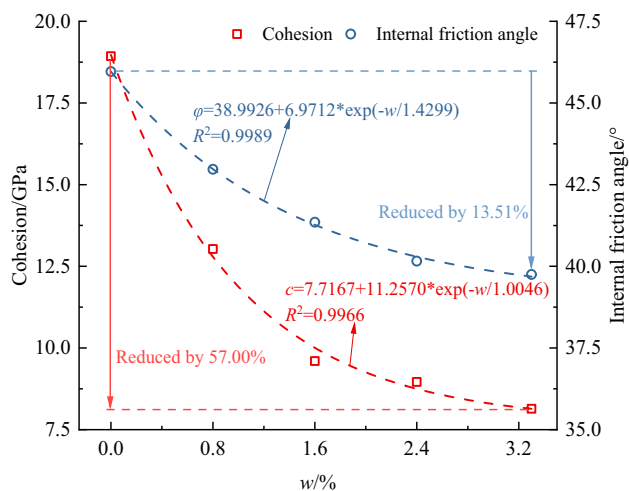


**Fig. 5** Relationship between sandstone cohesion and internal friction angle and water content

content on cohesion is greater than its effect on the angle of internal friction (Fig. 5).

### 2.5 Creep Experiment Method

Creep tests were conducted using the five-channel rheological testing system (Fig. 2) at the State Key Laboratory of Geomechanics and Deep Underground Engineering (SKL-GDUE) following the short-term strength experiments. The system includes five sets of electric control cylinders and servo oil cylinders, with a maximum axial pressure of 600 kN and a lateral pressure range of 0–60 MPa, and can perform creep tests on five samples simultaneously. An inner sleeve was used to isolate the sample from the loading fluid, and Vaseline was applied to seal the interface between the upper and lower loading heads to ensure the stability of the water content during the experiment. The confining pressure was loaded to the predetermined value at a rate of 0.1 MPa/s, and the samples were loaded to the target stress at a constant rate of 0.5 kN/s. The target stress was held for a specified time under a constant deformation, and the creep time for each level was designed to be 24 h until the sample experienced creep failure. Table 1 shows the experimental scheme performed for this study.

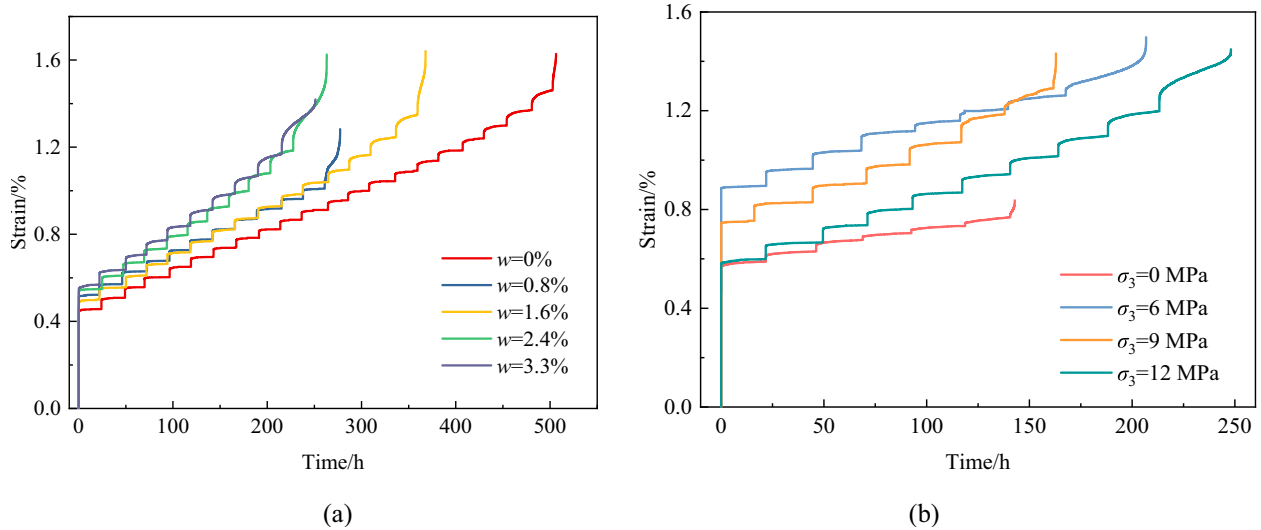
### 3 Creep Experiment Results

Figure 6 displays the graded loading creep curves of sandstone at various water contents and confining pressure. The overall strain exhibits a stepwise increase with time, with an instantaneous strain produced upon incremental load application, followed by decelerated creep and steady-state creep stage until the next incremental load is applied. At the

**Table 1** Creep load classification

| Sample number | w/% | $\sigma_3$ /MPa | Graded loading stress/MPa |                       |
|---------------|-----|-----------------|---------------------------|-----------------------|
|               |     |                 | Initial stress/MPa        | Stress difference/MPa |
| DR-10         | 0   | 0               | 18                        | 2.25                  |
| DR-11         | 0.8 |                 |                           |                       |
| DR-12         | 1.6 |                 |                           |                       |
| DR-13         | 2.4 |                 |                           |                       |
| DR-14         | 3.3 |                 |                           |                       |
| SR-10         | 0   | 6               | 30                        | 4.5                   |
| SR-11         | 0.8 |                 |                           |                       |
| SR-12         | 1.6 |                 |                           |                       |
| SR-13         | 2.4 |                 |                           |                       |
| SR-14         | 3.3 |                 |                           |                       |
| SR-20         | 0   | 9               | 30                        |                       |
| SR-21         | 0.8 |                 |                           |                       |
| SR-22         | 1.6 |                 |                           |                       |
| SR-23         | 2.4 |                 |                           |                       |
| SR-24         | 3.3 |                 |                           |                       |
| SR-30         | 0   | 12              | 30                        |                       |
| SR-31         | 0.8 |                 |                           |                       |
| SR-32         | 1.6 |                 |                           |                       |
| SR-33         | 2.4 |                 |                           |                       |
| SR-34         | 3.3 |                 |                           |                       |

last loading stress level, the creep strain rapidly increases, ultimately entering the accelerated creep stage, with sample failure occurring. For instance, for a sandstone sample at saturation state ( $w = 3.3\%$ ) and a confining pressure of 9 MPa, the sample underwent eight stress levels before experiencing creep failure. The total creep time was approximately 162.9 h, and the accelerated creep failure occurred approximately 1.2 h after the last loading. The creep deformation under each loading level increases significantly with an increase in water content, as shown in Fig. 6a, indicating that water content can significantly enhance the creep deformation of sandstone and reduce its long-term strength, leading to creep failure at lower stress levels. Figure 6b illustrates that, under the same water content conditions, the maximum deformation of sandstone increases with an increase in confining pressure. Based on the results of short-term strength compression experiments and creep tests, the ratio of creep failure stress ( $\sigma_{cf}$ ) to compressive strength ( $\sigma_c$ ) of sandstone at various water contents and confining pressure was obtained, as shown in Table 2. Creep destructive stress refers to the value of the stress that the sample is subjected to when it undergoes creep deformation and eventual destruction under long-term stress. Compressive strength refers to the ability of the sample to resist damage under compression,



**Fig.6** Creep test curves of different water content and confining pressure: **a**  $\sigma_3=6$  MPa; **b**  $w=3.3\%$

which is the maximum stress that the sample can withstand in a one-way compression test.

The ratio of creep failure stress to compressive strength ranges from 0.66 to 0.98. The relationship between the creep failure stress and water content follows a negative exponential relationship, while that with confining pressure follows an exponential relationship, as shown in Fig. 7. At the same

time, we attempted to plot  $\sigma_{cf}/\sigma_c$  versus water content and confining pressure (Fig. 7c), and it can be observed that  $\sigma_{cf}/\sigma_c$  is minimized at a water content of 0% and a confining pressure of 0 MPa. The ratio increases with the increase in water content and confining pressure. At the maximum water content and confining pressure, the ratio shows a relative decrease.

**Table 2** Relationship between creep failure stress and compressive strength

| $\sigma_3$ /MPa | $w$ /% | $\sigma_c$ /MPa | $\sigma_{cf}$ /MPa | $\sigma_{cf}/\sigma_c$ |
|-----------------|--------|-----------------|--------------------|------------------------|
| 0               | 0      | 90.67           | 59.63              | 0.66                   |
|                 | 0.8    | 56.25           | 36.00              | 0.64                   |
|                 | 1.6    | 42.91           | 36.00              | 0.84                   |
|                 | 2.4    | 37.30           | 29.25              | 0.78                   |
|                 | 3.3    | 33.74           | 27.00              | 0.80                   |
| 6               | 0      | 130.20          | 104.30             | 0.80                   |
|                 | 0.8    | 93.00           | 84.00              | 0.90                   |
|                 | 1.6    | 70.90           | 70.50              | 0.98                   |
|                 | 2.4    | 63.50           | 59.25              | 0.93                   |
|                 | 3.3    | 58.00           | 52.50              | 0.91                   |
| 9               | 0      | 141.11          | 124.50             | 0.88                   |
|                 | 0.8    | 98.26           | 84.00              | 0.85                   |
|                 | 1.6    | 80.15           | 78.00              | 0.97                   |
|                 | 2.4    | 72.06           | 70.50              | 0.98                   |
|                 | 3.3    | 67.13           | 57.00              | 0.85                   |
| 12              | 0      | 152.00          | 124.50             | 0.82                   |
|                 | 0.8    | 107.60          | 97.50              | 0.91                   |
|                 | 1.6    | 86.80           | 79.50              | 0.92                   |
|                 | 2.4    | 80.59           | 75.00              | 0.93                   |
|                 | 3.3    | 76.30           | 70.50              | 0.92                   |

## 4 Effect of Water Damage on Creep Characteristics of Sandstone Under Triaxial Confinement

Using the Chen loading method (Chen et al. 1991; Lin et al. 2022), the full creep curve was transformed into graded loading creep curves, taking into account the memory effect of rock under loading. Figure 8 displays the creep curves of sandstone samples DR-10 ( $\sigma_3=0$  MPa  $w=0\%$ ) and SR-32 ( $\sigma_3=12$  MPa  $w=1.6\%$ ) as examples. The strain of the sandstone sample consists of instantaneous strain  $\epsilon_i$  and creep strain  $\epsilon_c$ , with the sample strain mainly being instantaneous strain under different stress levels. The creep characteristics of the sample are more significant under high stress levels, as shown in the figure.

### 4.1 Instantaneous Strain

The graded loading creep curves provide the instantaneous strain corresponding to each completed load level. By separating the instantaneous and creep strains during the creep process of sandstone samples, the regular curves of axial instantaneous and creep strains under different water contents and confining pressure were obtained, as shown in

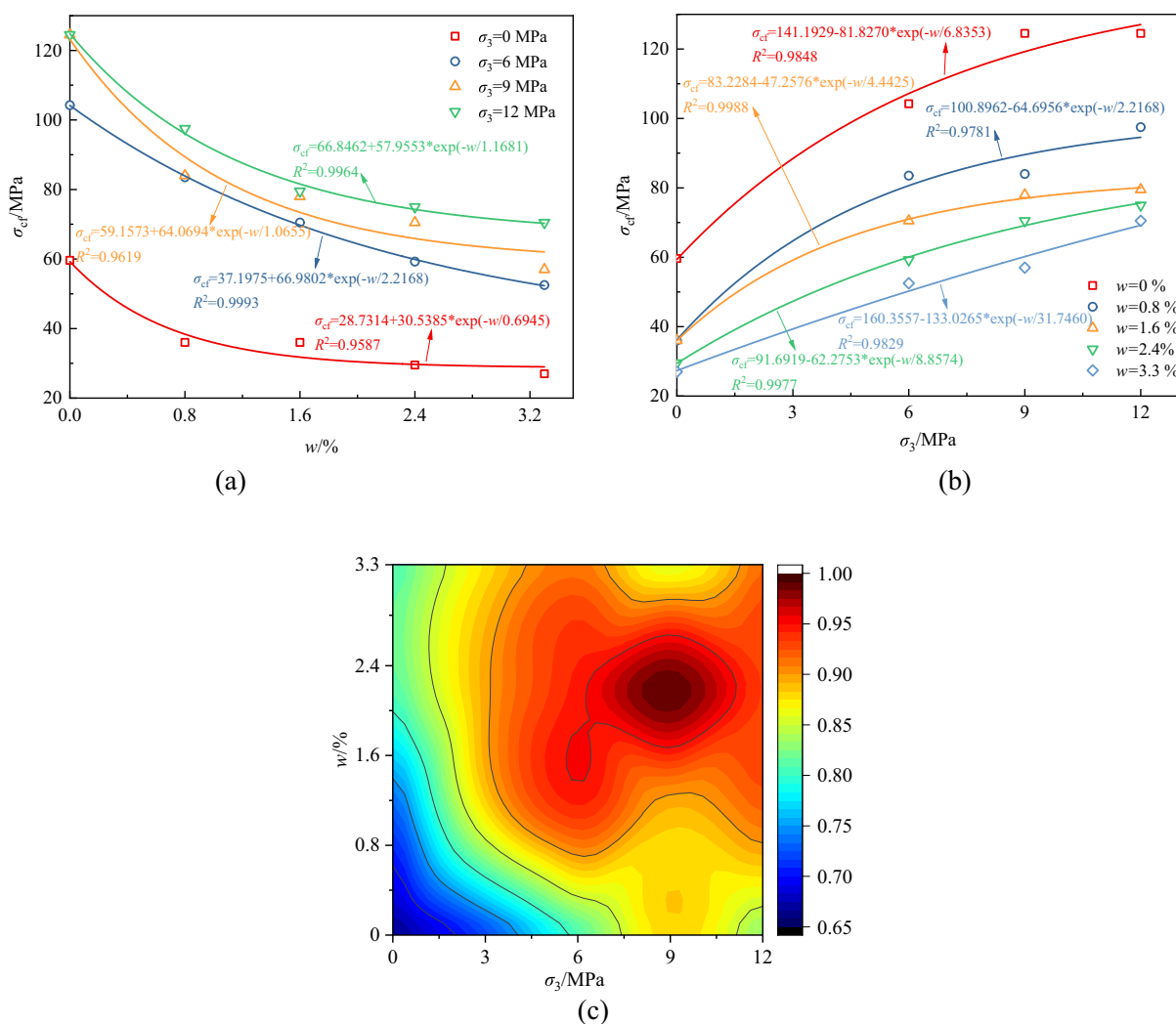


**Fig. 7** Relationships among creep failure stress ( $\sigma_{cf}$ ), water content and confining pressure: **a** water content; **b** confining pressure; **c**  $\sigma_{cf}/\sigma_c$  versus water content and confining pressure

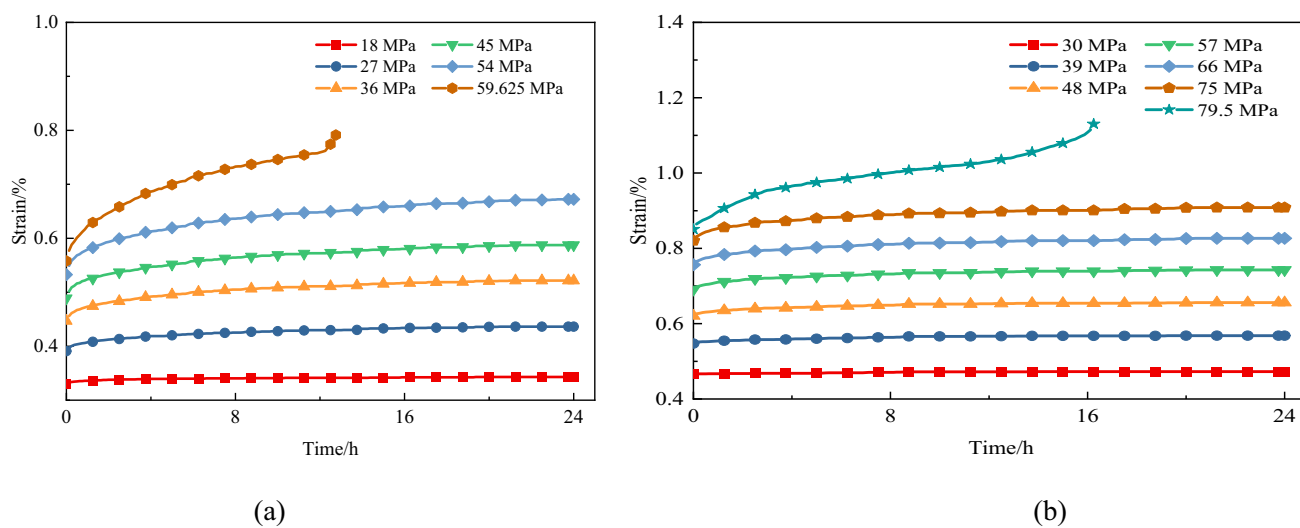


**Fig. 8** Creep curves of different samples under graded load: **a** DR-10 ( $\sigma_3 = 0 \text{ MPa}$ ,  $w = 0\%$ ); **b** SR-32 ( $\sigma_3 = 12 \text{ MPa}$ ,  $w = 1.6\%$ )



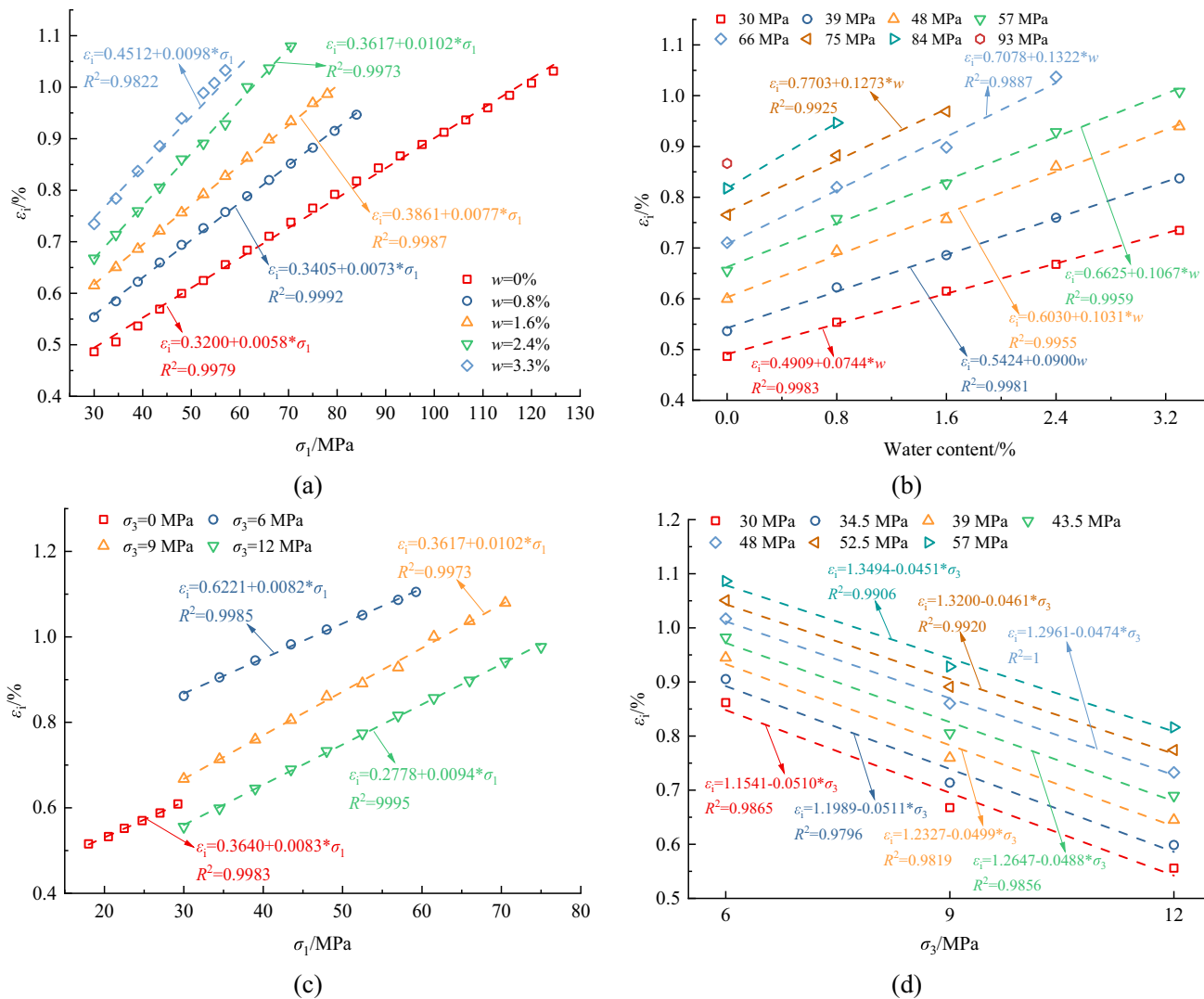


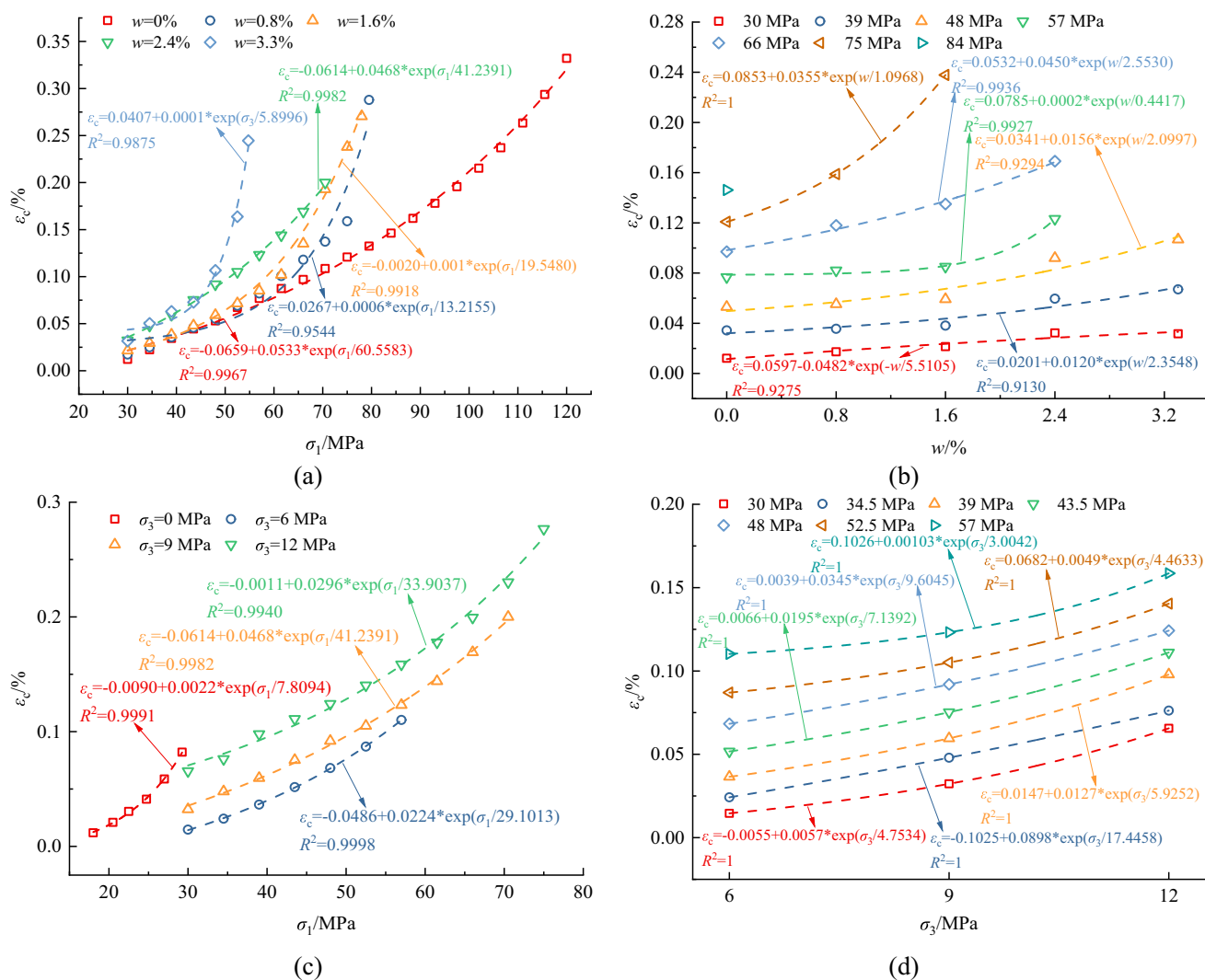
Fig. 9 Relationships among instantaneous strain, water content, and confining pressure: **a**  $\sigma_3=9$  MPa; **b**  $\sigma_3=9$  MPa; **c**  $w=2.4\%$ ; **d**  $w=2.4\%$

Fig. 9 and Fig. 10. For instance, samples with a confining pressure of 9 MPa and a water content of 2.4% were used as examples in this study.

As shown in Fig. 9a, the relationship between sandstone instantaneous strain and deviator stress at different water contents is linearly increasing. The curve slope of the saturated sample is larger, indicating that the reduction in elastic modulus due to water content allows saturated samples to produce more elastic deformation under the same stress difference. The effect of water on sandstone creep not only affects the initial instantaneous strain but also affects the elastic stage of the whole creep process. This phenomenon is due to the weakening of the internal structure and mineral composition of sandstone by water, reducing its strength and increasing the instantaneous strain under load. Comparing the instantaneous strains corresponding to water contents of 0% and 2.4%, the difference between

instantaneous strains gradually increases as the deviator stress increases. The influence of water content on sandstone instantaneous strain is related to deviator stress. As deviator stress increases, the influence of water content on sandstone instantaneous strain gradually increases. Figure 9b shows the linearly increasing relationship between sandstone instantaneous strain and water content for the same load. This phenomenon is mainly due to pore water weakening the bonding strength between particles, and internal pore water reducing the bonding ability of clay fillers, thereby weakening the strength of sandstone.

The linearly increasing relationship between sandstone instantaneous strain and deviator stress at different confining pressures is shown in Fig. 9c. Meanwhile, the linearly decreasing relationship between sandstone instantaneous strain and confining pressure for the same load is shown in Fig. 9d. As the confining pressure increases,



**Fig. 10** Relationships among creep strain, water content, and confining pressure: **a**  $\sigma_3=9\text{ MPa}$ ; **b**  $\sigma_3=9\text{ MPa}$ ; **c**  $w=2.4\%$ ; **d**  $w=2.4\%$

the instantaneous strain under each load level significantly decreases. The slope of the curve of the relationship between sandstone instantaneous strain and deviator stress under different confining pressures is not significantly different, and confining pressure mainly affects the initial instantaneous strain of sandstone, with little effect on the elastic stage of the whole creep process.

## 4.2 Creep Strain

The long-term deformation of soft rock is the main factor leading to large deformation and damage of the surrounding rock in the roadway. The effect of water in the roadway on the deformation of rock under geostress is particularly significant. Creep strain directly reflects the deformation of rock over time, and is calculated by determining the

difference between the strain at the completion of each load level and the strain at the beginning of the next load level.

Figure 10a shows the exponential growth relationship between sandstone creep strain and deviator stress under different water contents. The creep strain of sandstone is significantly affected by the level of deviator stress, and it increases with the increase of deviator stress. The growth amplitude of creep strain is small at low deviator stress, corresponding to a smaller slope of the curve. When the deviator stress level reaches a high level, there is an approximate inflection point on the curve, and then, it increases rapidly. With the increase of water content, the total creep time gradually decreases. Figure 10b shows the exponential growth relationship between sandstone creep strain and water content for the same load. As the confining pressure increases, the instantaneous strain under each

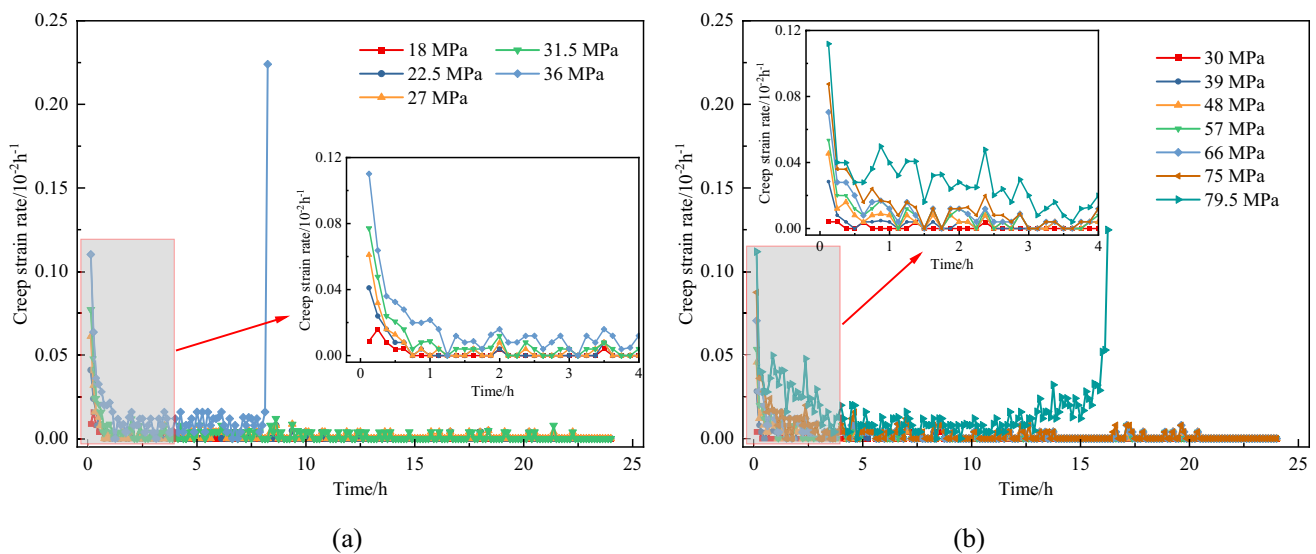


Fig. 11 Graded creep strain rate curve: **a** DR-11 ( $\sigma_3=0$  MPa  $w=0.8\%$ ); **b** SR-32 ( $\sigma_3=12$  MPa  $w=1.6\%$ )

load level significantly increases. This phenomenon is due to the random development of internal cracks in sandstone, which are enlarged by water under the action of confining pressure. Figure 10c shows the exponential growth relationship between sandstone creep strain and deviator stress under different confining pressures. Figure 10d shows the exponential growth relationship between sandstone instantaneous strain and confining pressure for the same load. As the confining pressure increases, the creep strain under each load level significantly increases.

Under the same confining pressure, the creep strain increases with the increase of water content. When the deviator stress is lower than the creep stress threshold, the creep strain generated by high confining pressure is larger, indicating that before the creep failure of sandstone, the greater the confining pressure, the more likely it is to produce creep strain. In summary, the greater the confining pressure and water content, the more obvious the time-dependent deformation characteristics of sandstone.

### 4.3 Creep Strain Rate

To further investigate the creep deformation law and obtain the creep rate curves under various load levels, as shown in Fig. 11, this paper presents the creep rate curves of sandstone samples DR-11 ( $\sigma_3=0$  MPa  $w=0.8\%$ ) and SR-32 ( $\sigma_3=12$  MPa  $w=1.6\%$ ). Creep rate is an important indicator for studying the creep characteristics of rocks and is also an important basis for distinguishing the different stages of creep.

According to the creep rate, rock creep can be divided into three stages: attenuation creep (Stage I), steady-state creep (Stage II), and accelerated creep (Stage III), as shown

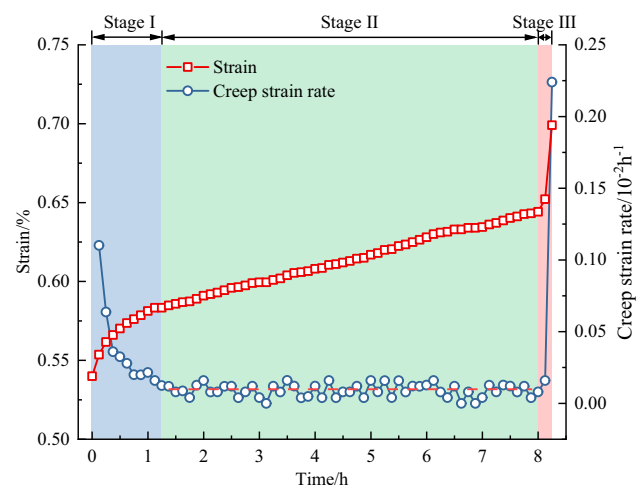
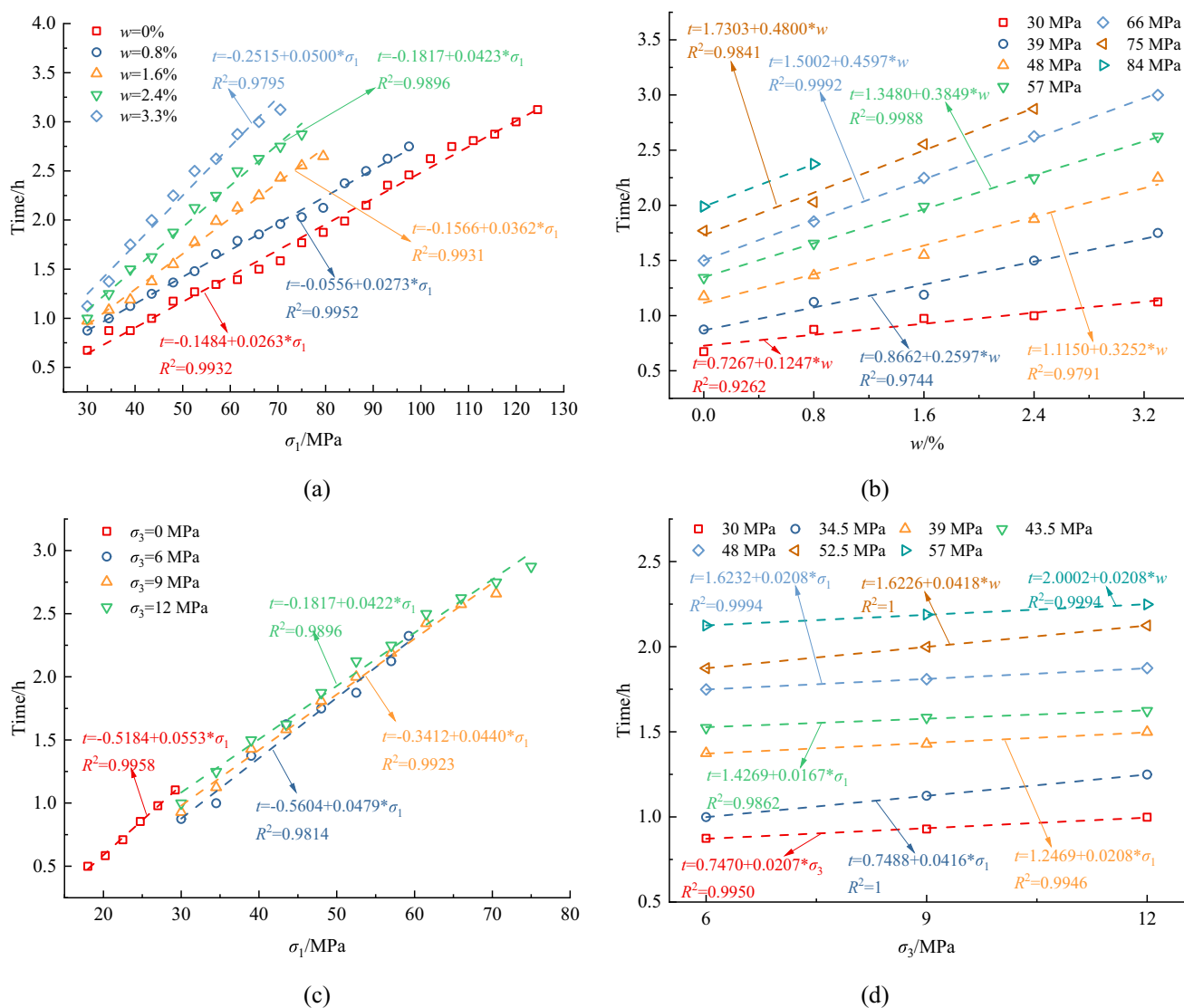


Fig. 12 Division of rock creep stage (DR-11 ( $\sigma_3=0$  MPa  $w=0.8\%$ ))

in Fig. 12 (using sample DR-11 as an example). From Fig. 12, it can be seen that the creep rate curve shows the characteristics of attenuation creep and steady-state creep. In each load stage, the creep rate of the attenuation creep stage reaches a relatively stable range within a certain period of time. When the load exceeds the creep failure stress, the sandstone not only undergoes attenuation creep and steady-state creep stages, but also undergoes an accelerated creep stage, in which the creep rate nonlinearly increases with time and the creep deformation rapidly increases. It can be found that the time occupied by the three creep stages is different, and the steady-state creep stage has the longest time and dominates the entire creep process, while the time occupied by the attenuation creep and accelerated creep stages is very short. Therefore, studying the creep rate variation law during



**Fig. 13** Time variation of attenuation creep stage of sandstone specimens: **a**  $\sigma_3 = 12$  MPa; **b**  $\sigma_3 = 12$  MPa; **c**  $w = 2.4\%$ ; **d**  $w = 2.4\%$

the creep process is of great significance for understanding the creep characteristics of sandstone.

Figure 13 illustrates the pattern of change in the time of attenuation creep phase of sandstone samples. This paper demonstrates the relationship between the attenuation creep stage time and deviator stress of sandstone at different water contents, using the sandstone sample with a confining pressure of 12 MPa and a water content of 2.4% as an example.

Figure 13a shows that the attenuation creep stage time linearly increases with deviator stress, and the curve slope of the sample with a higher water content is larger. The attenuation creep stage time increases more significantly as the water content increases. Comparing the attenuation creep stage time corresponding to water contents of 0% and 3.3%, the difference between the attenuation creep stage time gradually increases with the increase of deviator stress. The

effect of water content on the attenuation creep stage time is related to deviator stress, and as deviator stress increases, the influence of water content on the attenuation creep stage time of sandstone gradually increases. Figure 13b shows a linear increase in the attenuation creep phase time with increasing water content. The larger the load, the steeper the attenuation creep slope, and the longer the attenuation creep stage time.

Figure 13c and Fig. 13d illustrates the relationship between attenuation creep phase time, stress, and confining pressure for sandstones at different confining pressures. The attenuation creep stage time shows an exponential increase with deviator stress and confining pressure. When the water content is constant, the slope of the attenuation creep stage time and deviator stress curve under different confining pressures is roughly the same, indicating that the effect of

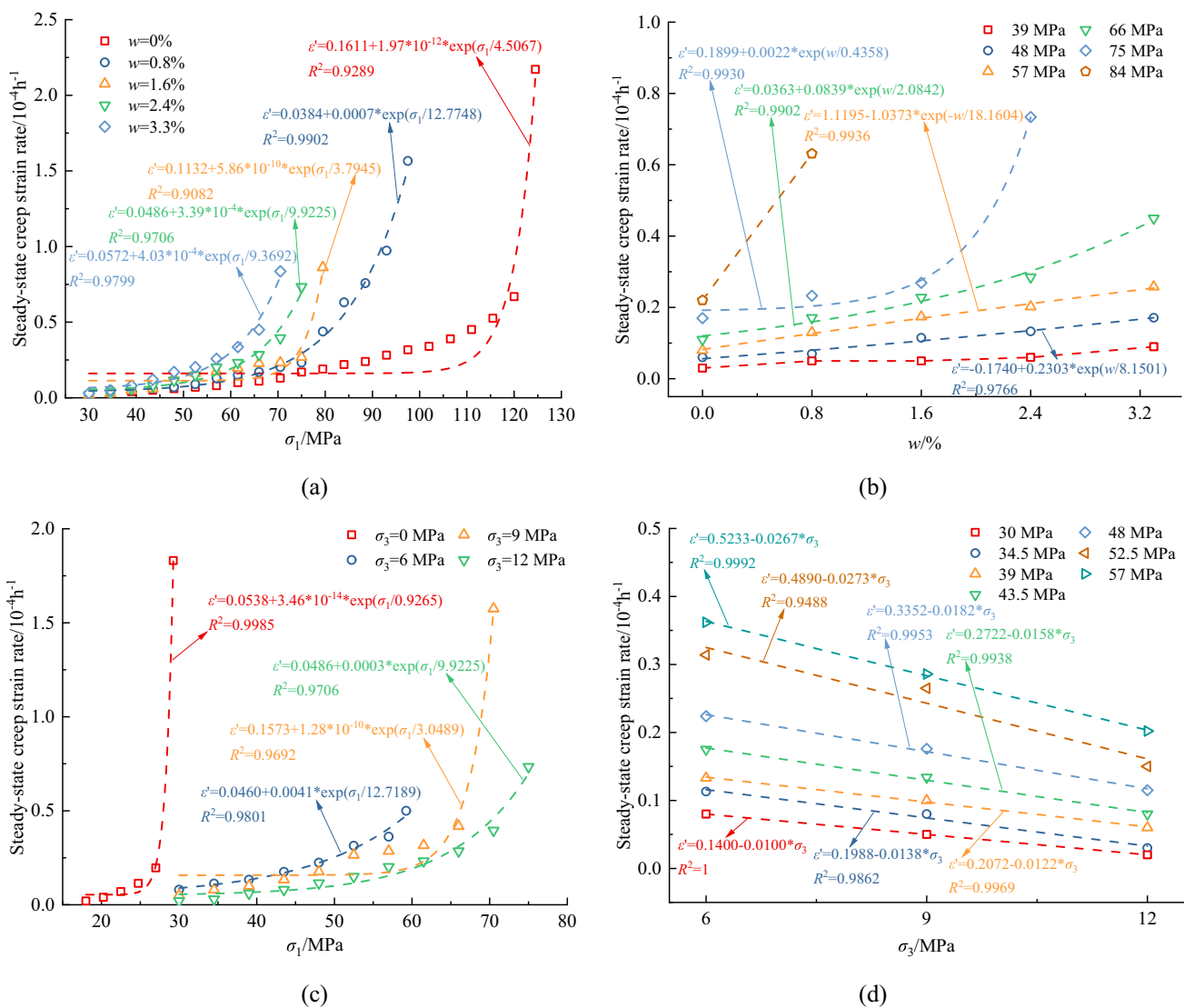
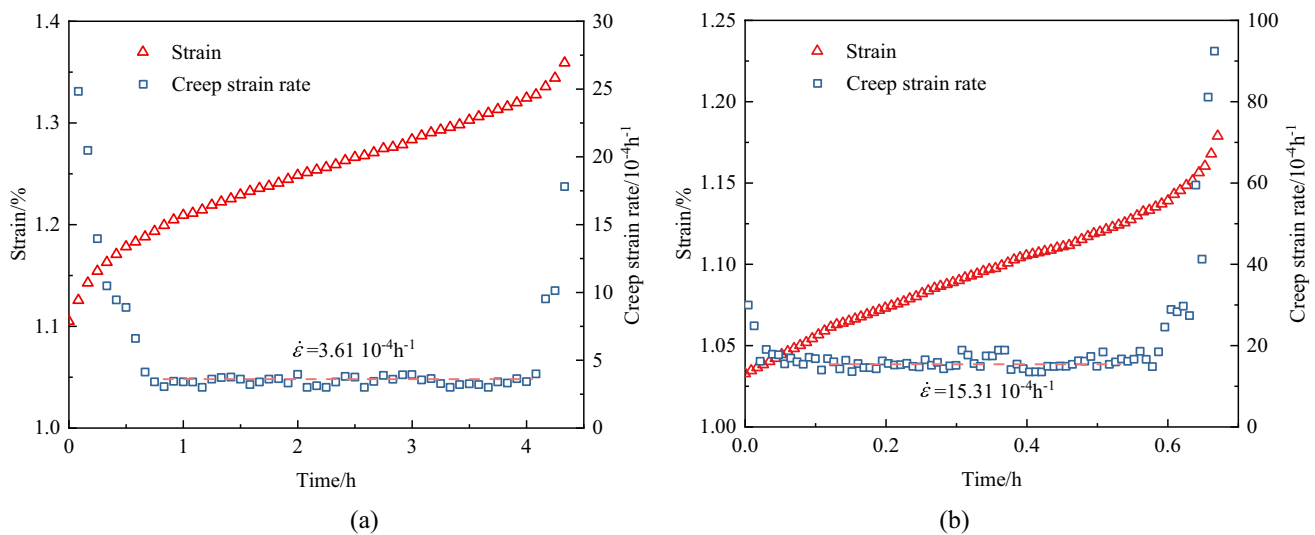


Fig. 14 Steady-state creep rate of sandstone under different water content and confining pressure: a  $\sigma_3 = 12$  MPa; b  $\sigma_3 = 12$  MPa; c  $w = 2.4\%$ ; d  $w = 2.4\%$

confining pressure on the attenuation creep stage time is independent of deviator stress. Similarly, the slope of the attenuation creep stage time and confining pressure curve under the same load is roughly the same, indicating that the effect of deviator stress on the attenuation creep stage time is independent of confining pressure.

This study investigates the deformation patterns of the steady-state creep stage, which is characterized by the steady-state creep rate, an essential indicator for distinguishing between different creep stages. Figure 14 illustrates the steady-state creep rate curves of sandstone samples subjected to graded loading under varying confining pressures and water contents. Using the sandstone sample with a confining pressure of 12 MPa and a water content of 2.4% as an example.

Figure 14a and Fig. 14b demonstrates the exponential growth relationship between the steady-state creep rate and the deviator stress and water content of sandstone. Similar to the strain deformation patterns, the steady-state creep rate remains low in the initial stages of stress and gradually increases as the stress level rises, eventually entering a nonlinear growth phase. Under the same deviator stress, the steady-state creep rate increases with an increase in water content. The creep rate is more significant when the load level is higher and reaches the steady-state creep stage. Figure 14c and Fig. 14d exhibits the exponential growth relationship between the steady-state creep rate and the deviator stress and confining pressure of sandstone samples under different confining pressures. The steady-state creep rate increases exponentially with



**Fig. 15** Accelerated creep curve of sandstone: **a** SR-13 ( $\sigma_3 = 6$  MPa  $w = 2.4\%$ ); **b** SR-24 ( $\sigma_3 = 9$  MPa  $w = 3.3\%$ )

deviator stress and is inversely proportional to the confining pressure. When the water content is 2.4%, the creep rate is almost zero at low deviator stresses. Under the same deviator stress, the difference in creep rate caused by varying confining pressures is not significant. The steady-state creep rate increases rapidly when the deviator stress exceeds the stress threshold. Under the same deviator stress, the steady-state creep rate decreases gradually with an increase in confining pressure.

The results show that the exact timing for entering the accelerated creep stage has no obvious regularity with respect to the confining pressure and water content. However, it can be considered that the sandstone enters the accelerated creep stage when the axial creep strain reaches a certain threshold value, and from the results, it can be seen that the duration of the accelerated creep failure stage is closely related to the preceding steady-state creep stage before reaching this threshold value.

To analyze the variation characteristics of the creep rate in the three stages, we organized the curves of the creep rate with time at the last level of deviator stress. Figure 15 shows the curves for samples SR-13 ( $\sigma_3 = 6$  MPa  $w = 2.4\%$ ) and SR-24 ( $\sigma_3 = 9$  MPa  $w = 3.3\%$ ). The creep process of sandstone can be divided into three stages: attenuated creep, steady-state creep, and accelerated creep. Among these stages, the steady-state creep stage has the longest duration, while the accelerated creep stage has the shortest. Although the accelerated creep stage accounts for only a small part of the entire creep process, it is the most apparent. During this stage, the deformation

**Table 3** Triaxial steady-state creep rate and accelerated failure time of the last load

| $\sigma_3/\text{MPa}$ | $w/\%$ | $\dot{\epsilon}'/10^{-4} \text{ h}^{-1}$ | $t_a/\text{h}$ | $\epsilon_{ac}/10^{-4}$ |
|-----------------------|--------|--|----------------|-------------------------|
| 0                     | 0      | 0.73                                     | 0.75           | 0.55                    |
|                       | 0.8    | 0.34                                     | 1.87           | 0.63                    |
|                       | 1.6    | 1.74                                     | 0.42           | 0.73                    |
|                       | 2.4    | 1.83                                     | 0.42           | 0.77                    |
|                       | 3.3    | 2.57                                     | 0.25           | 0.64                    |
| Average value         | -      | -  | -              | 0.66                    |
| 6                     | 0      | 0.71                                     | 2.37           | 1.69                    |
|                       | 0.8    | 1.91                                     | 0.80           | 1.53                    |
|                       | 1.6    | 19.23                                    | 0.10           | 1.92                    |
|                       | 2.4    | 3.61                                     | 0.41           | 1.48                    |
|                       | 3.3    | 0.46                                     | 5.00           | 2.32                    |
| Average value         | -      | -  | -              | 1.79                    |
| 9                     | 0      | 0.68                                     | 3.20           | 2.18                    |
|                       | 0.8    | 0.46                                     | 5.25           | 2.42                    |
|                       | 1.6    | 0.72                                     | 2.12           | 1.51                    |
|                       | 2.4    | 1.57                                     | 1.42           | 2.23                    |
|                       | 3.3    | 15.30                                    | 0.13           | 1.96                    |
| Average value         | -      | -  | -              | 2.06                    |
| 12                    | 0      | 2.17                                     | 1.04           | 2.26                    |
|                       | 0.8    | 0.80                                     | 3.50           | 2.82                    |
|                       | 1.6    | 0.86                                     | 3.32           | 2.86                    |
|                       | 2.4    | 0.73                                     | 3.26           | 2.39                    |
|                       | 3.3    | 0.67                                     | 3.07           | 2.57                    |
| Average value         | -      | -  | -              | 2.58                    |

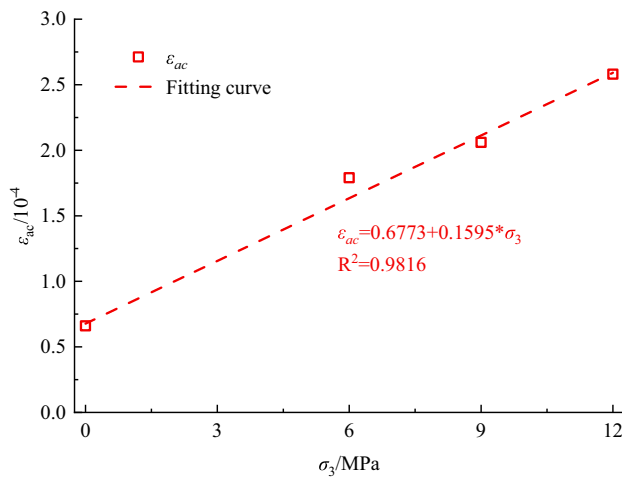


**Fig. 16** Relationship between strain parameters  $\epsilon_{ac}$  and confining pressure

and creep rate are the largest and fastest, respectively, but the time is the shortest. This ultimately leads to the final failure of the specimen, which is related to the large deformation and failure of the surrounding rock in practical engineering. The rapid increase of the creep rate during the accelerated creep stage is the macroscopic manifestation of the development of internal cracks in the sandstone. At this time, under the joint action of water and confining pressure, the rock undergoes accelerated damage, which reduces its bearing capacity, further accelerates the damage, and leads to the nonlinear and rapid increase of strain during this stage.

#### 4.4 Accelerated Creep Stage

To further investigate the influence of steady-state creep rate on the duration of accelerated creep before failure, the steady-state creep rate and duration of the accelerated creep stage under the final load are statistically recorded in Table 3. Additionally, a strain parameter  $\epsilon_{ac}$  was defined, expressed as the product of steady-state creep rate  $\epsilon'$  and the duration of the accelerated creep stage  $t_a$ , as shown in Eq. (3). This parameter numerically characterizes the strain value developed by the steady-state creep rate before the nonlinear strain growth occurs during the failure stage. Figure 16 shows the relationship between strain parameter  $\epsilon_{ac}$  and confining pressure, which exhibits a linear increase with confining pressure. This indicates that higher confining pressures have a greater influence of the steady-state creep rate on the duration of accelerated creep before failure.

$$\epsilon_{ac} = \epsilon' \cdot t_a \quad (3)$$

## 5 Discussion

### 5.1 The Influence of Water Content and Confining Pressure on Creep Characteristic Stress

To explore the impact of water on sandstone creep's viscoelastic–plastic deformation phase, we processed the complete creep dataset to eliminate instantaneous strain from applied stress. Through statistical analysis of the entire process, we derived equivalent time-dependent viscoelastic–plastic stress–strain curves, as depicted in Fig. 17a. The deformation process was categorized into three segments: viscoelastic, plastic, and nonlinear damage deformation, as illustrated in Fig. 17b. Analyzing the creep curve, we observed that with relatively low creep stress, sandstone enters the creep phase post-application of instantaneous load. Following a brief period of decelerated creep, strain stabilizes at a consistent level. After 24 h of creep, strain remains nearly constant, correlating with creep stress and depicted by the linear increase in Stage I. This process aligns with viscoelastic deformation theory. Upon surpassing a threshold stress, the equivalent time-dependent creep curve transitions into Stage II. Here, creep rate stabilizes post-deceleration, inducing plastic deformation. Despite 24 h of creep, the equivalent time-dependent creep curve maintains a linear increase, indicating proportional plastic deformation with creep stress. The critical stress demarcating Stages I and II is denoted by the yield limit  $\sigma_s$ . As stress escalates, strain exhibits nonlinear growth post-reaching a certain threshold, designating this critical stress as the long-term strength  $\sigma_l$ .

The critical strengths of samples with different moisture contents at different stages are recorded in Table 4. Figure 18 illustrates the evolution of various stresses with confining pressure and moisture content. It is evident that although moisture content reduces the absolute values of various strengths, confining pressure increases the values of these strengths to a certain extent. However, under the coupled effect of moisture content and confining pressure, there still exists a certain regularity in the stresses entering different deformation stages of creep. Therefore, in subsequent studies, absolute stress values will be converted into ratios of critical stresses. It can be observed that under the same confining pressure, the yield limit  $\sigma_s$  and long-term strength  $\sigma_l$  decrease exponentially with increasing moisture content. Whereas under the same moisture content, the  $\sigma_s$  and  $\sigma_l$  increase linearly with increasing confining pressure. Calculations reveal that the ratio of  $\sigma_s$  to  $\sigma_c$  ranges from 0.44 to 0.59, and the ratio of  $\sigma_l$  to  $\sigma_c$  ranges from 0.59 to 0.74.

In prior studies (Sun et al. 2021; Miao et al. 2023), water–rock interaction effects on surrounding rock properties were investigated using unpressurized water

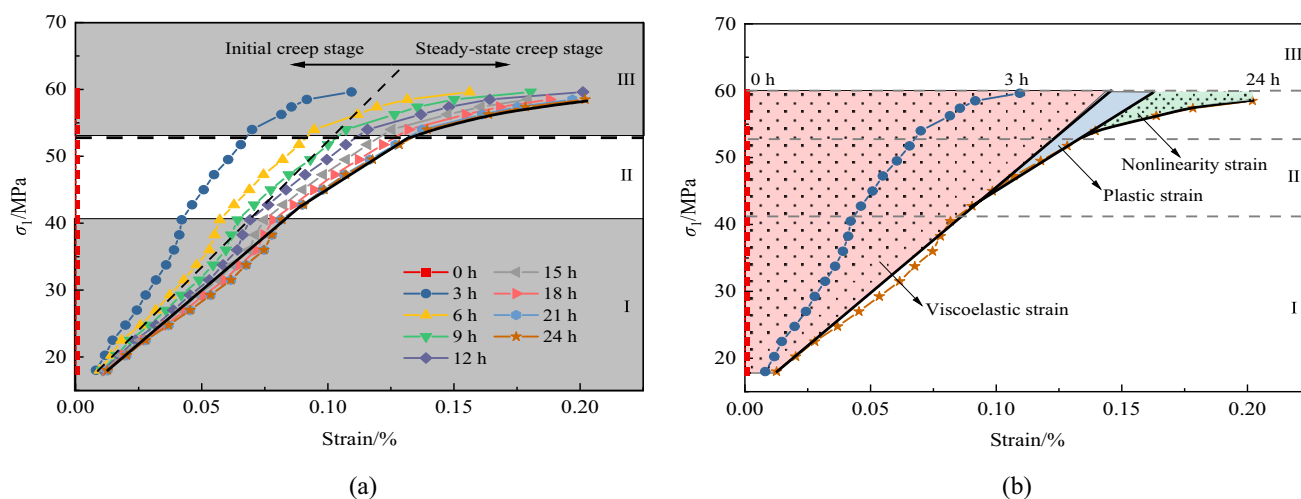


**Fig. 17** Isochronous viscoelastic-plastic stress–strain curve (DR-10 ( $\sigma_3=0$  MPa  $w=0\%$ )): **a** stress–strain curve; **b** deformation division

**Table 4** Failure stress, yield limit, and accelerated yield limit of sandstone creep test

| $\sigma_3$ /MPa | $w$ /% | $\sigma_c$ /MPa | $\sigma_s$ /MPa | $\sigma_s/\sigma_c$ | $\sigma_l$ /MPa | $\sigma_{as}/\sigma_c$ |
|-----------------|--------|-----------------|-----------------|---------------------|-----------------|------------------------|
| 0               | 0      | 90.67           | 40.5            | 0.44                | 54              | 0.59                   |
|                 | 0.8    | 56.25           | 31.5            | 0.56                | 37.13           | 0.66                   |
|                 | 1.6    | 42.91           | 22.5            | 0.52                | 29.25           | 0.68                   |
|                 | 2.4    | 37.30           | 20.25           | 0.54                | 25.88           | 0.69                   |
|                 | 3.3    | 33.74           | 18              | 0.53                | 24.75           | 0.73                   |
| Average value   | –      | –               | –               | 0.53                | –               | 0.70                   |
| 6               | 0      | 130.20          | 66              | 0.51                | 88.5            | 0.68                   |
|                 | 0.8    | 93.00           | (51)            | (0.55)              | 61.5            | 0.66                   |
|                 | 1.6    | 70.90           | 39              | 0.55                | 48.0            | 0.67                   |
|                 | 2.4    | 63.50           | 34.5            | 0.54                | 43.5            | 0.69                   |
|                 | 3.3    | 58.00           | 34.5            | 0.59                | 39.0            | 0.67                   |
| Average value   | –      | –               | –               | 0.55                | –               | 0.68                   |
| 9               | 0      | 141.11          | 70.5            | 0.50                | 93.0            | 0.67                   |
|                 | 0.8    | 98.26           | 52.5            | 0.53                | 61.5            | 0.62                   |
|                 | 1.6    | 80.15           | 38.8            | 0.50                | 55.6            | 0.72                   |
|                 | 2.4    | 72.06           | (39)            | (0.55)              | 52.5            | 0.74                   |
|                 | 3.3    | 67.13           | 39              | 0.58                | 43.5            | 0.65                   |
| Average value   | –      | –               | –               | 0.53                | –               | 0.68                   |
| 12              | 0      | 152.00          | 75              | 0.49                | 97.5            | 0.64                   |
|                 | 0.8    | 107.60          | 48              | 0.45                | 75.0            | 0.69                   |
|                 | 1.6    | 86.80           | 48              | 0.55                | 61.5            | 0.71                   |
|                 | 2.4    | 80.59           | 39              | 0.48                | 52.5            | 0.65                   |
|                 | 3.3    | 76.30           | 39              | 0.51                | 48.0            | 0.63                   |
| Average value   | –      | –               | –               | 0.50                | –               | 0.66                   |

The value in ( ) is the predicted value

absorption and uniaxial compression experiments. A Nuclear Magnetic Resonance (NMR) core analyzer examined dynamic changes in microporous rock structures during water–rock coupling. SEM analysis monitored

micromineral differences pre- and post-water absorption. Initially, in the dry state, rocks contained minimal crystallization and strongly bound water, resulting in few, mostly small pores, with limited pore size changes and negligible



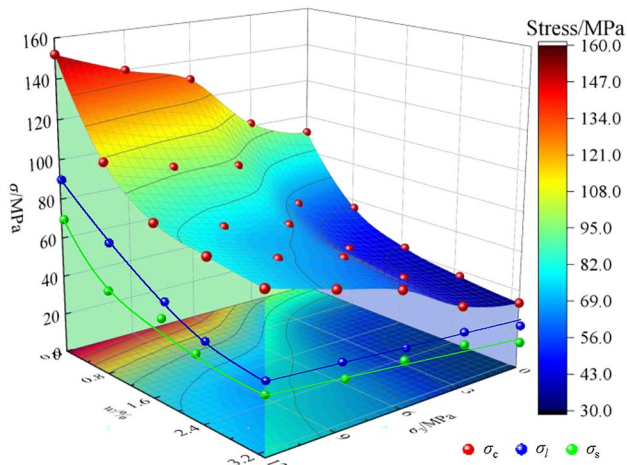


**Fig.18** Relationship between critical stress and confining pressure and water content

clay mineral structure alterations. As water absorption progressed, pore space increased, smaller pores closed, and larger ones expanded. Near saturation, clay particles expanded further, connecting with quartz particles and enlarging pores significantly. Clay mineral mud, coupled with quartz particle constraints, filled and compressed smaller pores, reducing nearby quartz particles. Under magnification, reductions in kaolinite flakes and interlayer

pore space were evident, weakening mineral structures due to cement dissolution or particle loss. Concurrently, swelling and dissolution of hydrophilic minerals accelerated sandstone water absorption and softening.

### 5.2 Effects of Water Content and Confining Pressure on Creep Failure Characteristics

Water alters the micro-pore structure of sandstone samples, impacting their ultimate failure characteristics. Concurrently, short-term strength compression experiments reveal confining pressure's role in restraining sandstone deformation, leading to variations in experimental outcomes. Thus, investigating sandstone failure modes under creep stress with varying water contents through indoor mechanical experiments is crucial. To enhance clarity in observing internal crack characteristics, representative failure samples underwent CT scanning, providing comprehensive CT images depicting the complete failure mode, as depicted in Fig. 19. The scanning equipment was a LIGHTSPEED 8-slice spiral CT scanner from General Electric, with a scanning time frequency of 0.5 s/3600 s, and an image reconstruction time of 0.167 s (512×512 matrix). CT image analysis software (CCTAS) was used to reconstruct the results and calculate the data.

Figure 19 shows the sandstone failure mode in this study, with the left side showing the short-term failure

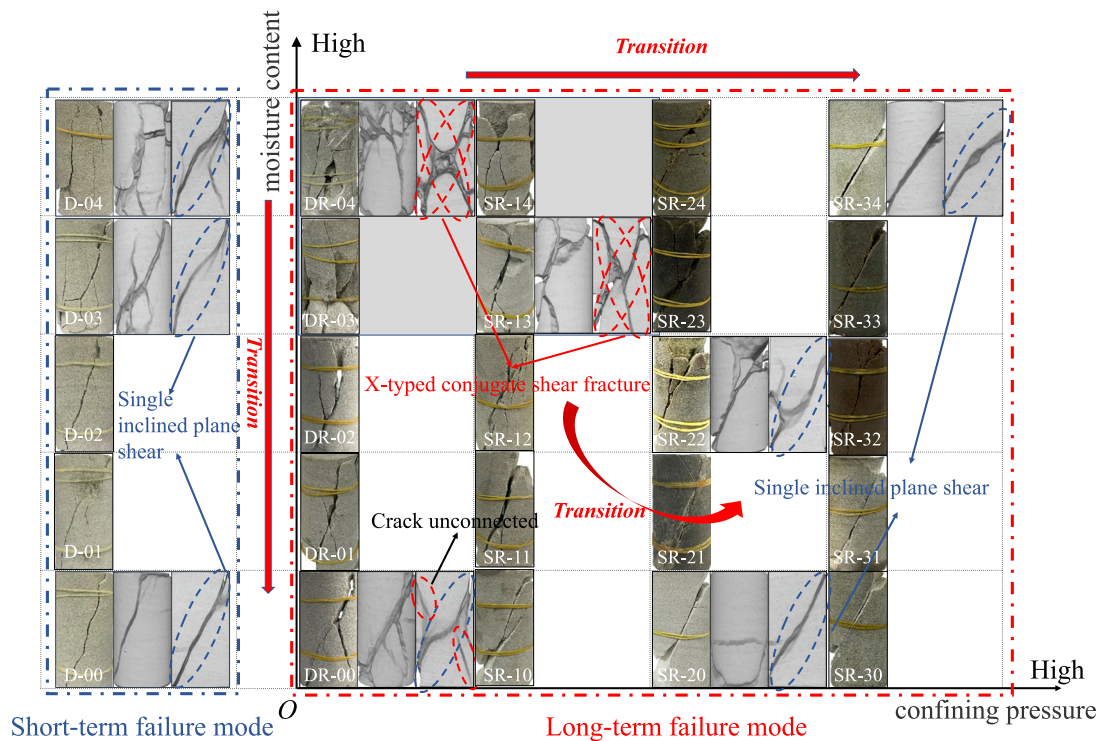


**Fig. 19** Relationship between failure mode and confining pressure and water content

mode. The failure mode of short-term strength compression experiments is controlled by a single oblique shear crack, and with the increase of water content, accompanying cracks and small cracks expand significantly. As confining pressure exists, the expansion of small cracks under triaxial compression is limited, resulting in a failure mode dominated by a single shear crack.

The right side of Fig. 19 shows the long-term failure mode of the sandstone in this study. When confining pressure is 0 MPa and the water content is relatively low, the failure of the sample is controlled by shear cracks. Although the failure mode of creep experiments is also controlled by shear cracks, there are significant differences in crack extension compared with short-term failure. Due to the slow expansion of cracks under long-term stress, there are more small cracks and accompanying cracks in the sample. In samples with higher water content, the fragmentation is more complete, and vertical surface cracks appear, with "X-shaped" conjugate shear cracks appearing from the middle of the internal cracks. At the same time, the characteristics of long-term sandstone failure under applied confining pressure were analyzed, and the failure mode was also dominated by shear failure, but the degree of fragmentation was smaller than that of uniaxial creep failure, and there were also fewer surface tensile cracks in higher water content samples. With the increase of confining pressure, the deformation failure is increasingly controlled by a single shear plane, and the development of small cracks is not obvious when the water content is relatively low. When the water content is high, there is an expansion of micro-cracks. With further increase of confining pressure, the influence of water content on the failure mode is small, and the development of small cracks is not obvious.

Based on the research analysis, it is suggested that there are two ways to reduce the long-term damage caused by rock creep in underground engineering. The first way is to isolate underground water and minimize contact between the rock and the water, which reduces the long-term strength of the rock and rock creep deformation. The second way is to use high pre-stress support, which applies confining pressure to the surrounding rock after excavation, so that the unstable rock mass remains in a triaxial stress state, thereby reducing the softening effect of water–rock coupling on the rock's ultimate strength.

## 6 Conclusions

After issues at Wanfu Coal Mine, sandstone samples from the –950 horizontal pumping station tunnel were analyzed. Short-term strength compression and creep experiments

were conducted on samples with different water contents. The experimental results are summarized as follows:

- 1) The relationship between water content and the mechanical properties of sandstone has been elucidated. It was observed that as water content increases, there is an exponential decrease in both short-term compressive strength and elastic modulus of sandstone. Under confining pressures of 0 MPa and 12 MPa, the compressive strength decreased from 90.67 MPa and 152.02 MPa in the dry state to 33.74 MPa and 76.29 MPa in the saturated state. Moreover, the influence of confining pressure on radial deformation and compressive strength was noted, with confining pressure exhibiting a linear increase effect. Micro-cohesion and internal friction angle of sandstone were found to decrease exponentially with water content, with cohesion being notably more affected. Additionally, the stress level of creep failure was found to be inversely correlated with water content and exponentially correlated with confining pressure, indicating the complex interplay between these factors in governing sandstone behavior.
- 2) Under high confining pressure conditions, increased water content was found to induce the formation of random internal cracks within the sandstone. The relationship between stress and various deformation parameters was investigated, revealing linear trends in instantaneous strain and decay creep stage time with stress, while creep strain and steady-state creep rate exhibited exponential trends. Furthermore, higher water content led to a more pronounced increase in instantaneous strain and decay creep stage time under constant confining pressure. The interplay of water content and confining pressure further influenced the creep behavior, with distinct trends observed in instantaneous strain, creep strain, decay creep stage time, and steady-state creep rate.
- 3) The deformation process of sandstone was characterized by a time-constant viscoelastic–plastic stress–strain curve, delineating three distinct stages: viscoelastic deformation, plastic deformation, and nonlinear acceleration. The critical strength (yield limit, long-term strength) entering different stages is obtained, and it can be found that the ratio of compressive strength remains stable between 0.44–0.59 and 0.59–0.74. Additionally, the strain parameter  $\varepsilon_{ac}$  was established as a predictor of accelerated creep failure time, showing a linear relationship with confining pressure irrespective of water content.
- 4) The failure modes of sandstone under varying conditions were investigated, with short-term failure primarily occurring through single oblique shear failure, accompanied by minor cracks that increased with water content. Long-term failure under low confining pressure and high

water content conditions exhibited an "X-shaped" conjugate shear failure mode due to extensive crack development. However, as confining pressure increased and water content decreased, the failure mode transitioned to single oblique shear failure. The implementation of groundwater isolation measures and the application of high confining pressure were identified as effective strategies for mitigating adverse impacts on structural integrity in onsite engineering projects, ensuring the integrity of structures throughout the construction process.

**Acknowledgements** This work was supported by the National Natural Science Foundation of China (Grant Nos. 52174096 and 52304110) and Henan International Joint Laboratory of Dynamics of Impact and Disaster of Engineering Structures, Nanyang Institute of Technology (Grant No. LDIDES-KF2022-02-05).

**Funding** National Natural Science Foundation of China, 52174096, Xiao Ming Sun, 52304110, Chengyu Miao, Fundamental Research Funds for the Central Universities, 2022YJSSB03, Xiao Ming Sun, Henan International Joint Laboratory of Dynamics of Impact and Disaster of Engineering Structures, Nanyang Institute of Technology, LDIDES-KF2022-02-05, Chengyu Miao

**Data availability** The raw/processed data required to reproduce the above findings cannot be shared at this time as the data also forms part of an ongoing study.

## Declarations

**Conflict of interest** The authors declare that they have no known competing financial interests or personal relationships that could have appeared to influence the work reported in this paper.

## References

- Chen ZJ, Kang WF, Huang JF (1991) Locked in stresses, creep and dilatancy of rocks, and constitutive equations. *Chin J Rock Mech Eng* 4:299–312
- Chen CF, Xu T, Heap MJ, Baud P (2018) Influence of unloading and loading stress cycles on the creep behavior of Darley Dale Sandstone. *Int J Rock Mech Min Sci* 112:55–63
- Chen PZ, Tang SB, Liang X, Zhang YJ, Tang CN (2021) The influence of immersed water level on the short- and long-term mechanical behavior of sandstone. *Int J Rock Mech Min Sci* 138:104631
- Chen GB, Li Y, Li T, Zhang GH (2023) Experimental study on the mechanical properties of intermittent jointed sandstone considering water–rock interaction and confining pressure effect. *B Eng Geol Environ* 82(4):113
- Damjanac B, Fairhurst C (2010) Evidence for a long-term strength threshold in crystalline rock. *Rock Mech Rock Eng* 43:513–531
- Deng HF, Zhou ML, Li JL, Sun XS, Huang YL (2016) Creep degradation mechanism by water–rock interaction in the red-layer soft rock. *Arab J Geosci* 9:1–12
- Fabre G, Pellet F (2006) Creep and time-dependent damage in argillaceous rocks. *Int J Rock Mech Min Sci* 43(6):950–960
- Fu TF, Xu T, Meredith PG, Mitchell TM, Heap MJ, Nara Y (2021) A meso-mechanical approach to time-dependent deformation and fracturing of partially saturated sandstone. *Int J Rock Mech Min Sci* 145:104840
- Gao Y, Wong LNY, Gao F (2015) Finite deformation analysis on sandstone subjected to thermo-hydro-mechanical (THM) coupling. *Rock Mech Rock Eng* 48:159–177
- Hawkins AB, Ulusay R, Hudson JA (2009) The complete ISRM suggested methods for rock characterisation, testing and monitoring. *Bull Eng Geol Environ* 68(2):287–288
- He MC, Wang Q (2023) Rock dynamics in deep mining. *Int J Min Sci Techno* 33(9):1065–1082
- Heap MJ, Baud P, Meredith PG (2009) Influence of temperature on brittle creep in sandstones. *Geophys Res Lett* 36(19):L19305
- Huang P, Zhang JX, Spearing AJS, Chai J, Dong CW (2021) Experimental study of the creep properties of coal considering initial damage. *Int J Rock Mech Min Sci* 139:104629
- Kang HP, Gao FQ, Xu G, Ren HW (2023) Mechanical behaviors of coal measures and ground control technology for China's deep coal mines-A review. *J Rock Mech Geotech Eng* 15(1):37–65
- Li YS, Xia CC (2000) Time-dependent tests on intact rocks in uniaxial compression. *Int J Rock Mech Min Sci* 37(3):467–475
- Li DJ, Wang GL, Han LQ (2011) Analysis of microscopic pore structures of rocks before and after water absorption. *Min Sci and Techno* 21(2):287–293
- Li F, You S, Ji HG, Elmo D, Wang HT (2020) Strength and energy exchange of deep sandstone under high hydraulic conditions. *J Cent South Univ* 27(10):3053–3062
- Li BY, Yang FW, Du PZ, Liu ZH (2022) Study on the triaxial unloading creep mechanical properties and creep model of shale in different water content states. *B Eng Geol Environ* 81(10):420
- Lin HX, Zhang QY, Zhang LY, Duan K, Xue TE, Fan QH (2022) The influence of water content on the time-dependent mechanical behavior of argillaceous siltstone. *Rock Mech Rock Eng* 55(7):3939–3957
- Liu DF, Yan WX, Yan S, Kang QR (2021) Study on the effect of axial and hydraulic pressure coupling on the creep behaviors of sandstone under multi-loading. *B Eng Geol Environ* 80:6107–6120
- Mei J, Yang L, Sheng XC, Ma XJ, Sui B, Yang WM (2021) An experimental and theoretical investigation of time-dependent cracking and creep behavior of rocks under triaxial hydro-mechanical coupling. *Theor Appl Fract Mech* 115:103046
- Miao CY, Yang L, Xu YZ, Yang K, Sun XM, Jiang M, Zhao WC (2021) Study on strength softening experiment and micro-mechanism of sandstone based on nuclear magnetic resonance. *Chin J Rock Mech Eng* 40(11):2189–2198
- Miao CY, Zhu MQ, Jiang M, Qi ZM, Li ZH, Sun XM (2023) Experimental study on the evolution of micropore structure softened by nonpressure water absorption strength of sandstone. *J Porous Media* 26(3):73–86
- Nara Y, Tanaka M, Harui T (2017) Evaluating long-term strength of rock under changing environments from air to water. *Eng Fract Mech* 178:201–211
- Ngwenya BT, Main IG, Elphick SC, Crawford BR, Smart BG (2001) A constitutive law for low-temperature creep of water-saturated sandstones. *J Geophys Res: Solid Earth* 106(B10):21811–21826
- Pan XK, Zhou XP (2022) Damage analysis of sandstone during the creep stage after high-temperature heat treatment based on NMR technology. *Rock Mech Rock Eng* 55(12):7569–7586
- Roy DG, Singh TN, Kodikara J, Das R (2017) Effect of water saturation on the fracture and mechanical properties of sedimentary rocks. *Rock Mech Rock Eng* 50:2585–2600
- Su QQ, Ma QY, Ma DD, Yuan P (2021) Dynamic mechanical characteristic and fracture evolution mechanism of deep roadway sandstone containing weakly filled joints with various angles. *Int J Rock Mech Min Sci* 137:104552

- Sun XM, Miao CY, Jiang M, Zhang Y, Yang L, Guo B (2021) Experimental and theoretical study on creep behaviors of sandstone with different moisture contents based on modified Nishihara model. *Chin J Rock Mech Eng* 40(12):2411–2420
- Sun XM, Jiang M, Miao CY, Wang J, Zhang JX (2023a) Study on large deformation and failure mechanism of deep buried stratified slate tunnel and control strategy of high constant resistance anchor cable. *Eng Fail Anal* 144:106953
- Sun XM, Jiang M, Wang XB, Zang JC, Gao X, Miao CY (2023b) Experimental study on creep mechanical properties of sandstone with different water contents in Wanfu coal mine. *Rock Soil Mech* 44(3):624–636
- Sun XM, Shi FK, Luan ZQ, Yang L, Ding JX, He LS, Zhang Y (2023c) Constitutive model and microscopic mechanism for sandstone strength softening damage. *Rock Mech Rock Eng* 56(1):797–813
- Sun XM, Shi FK, Ding JX, Tao ZG, Zhang Y, Miao CY, Cui L (2023d) Study on microscopic mechanism and failure mode of water–rock coupling in fine sandstone under uniaxial compression. *Rock Mech Rock Eng* 56(9):6823–6842
- Tang SB, Yu CY, Heap MJ, Chen PZ, Ren YG (2018) The influence of water saturation on the short- and long-term mechanical behavior of red sandstone. *Rock Mech Rock Eng* 51:2669–2687
- Tang SB, Li JM, Ding S, Zhang LT (2022) The influence of water-stress loading sequences on the creep behavior of granite. *B Eng Geol Environ* 81(11):482
- Tang MY, Gao MZ, Li SW, Yang BG, Tang RF, Li F, Liu JJ (2023) Failure behavior and energy evolution characteristics of deep roadway sandstone under different microwave irradiation modes. *J Cent South Univ* 30(1):214–226
- Tian HM, Chen WZ, Yang DS, Gong Z (2015) Experimental and numerical analysis of the time-dependent behaviour of argillaceous red sandstone under high in situ stress. *B Eng Geol Environ* 74:567–575
- Tran NT, Do DP, Hoxha D, Vu MN, Armand G (2021) Kriging-based reliability analysis of the long-term stability of a deep drift constructed in the Callovo-Oxfordian claystone. *J Rock Mech Geotech Eng* 13(5):1033–1046
- Vasarhelyi B, Ván PJEG (2006) Influence of water content on the strength of rock. *Eng Geol* 84(1–2):70–74
- Vergara MR, Triantafyllidis T (2016) Influence of water content on the mechanical properties of an argillaceous swelling rock. *Rock Mech Rock Eng* 49:2555–2568
- Wasantha PLP, Ranjith PG (2014) Water-weakening behavior of Hawkesbury sandstone in brittle regime. *Eng Geol* 178(8):91–100
- Wong LNY, Jong MC (2014) Water saturation effects on the Brazilian tensile strength of gypsum and assessment of cracking processes using high-speed video. *Rock Mech Rock Eng* 47:1103–1115
- Wu JY, Feng MM, Yu BY, Zhang WL, Ni XY, Han GS (2018) Experimental investigation on dilatancy behavior of water-saturated sandstone. *Int J Min Sci Techno* 28(2):323–329
- Yan BQ, Guo QF, Ren FH, Cai MF (2020) Modified Nishihara model and experimental verification of deep rock mass under the water–rock interaction. *Int J Rock Mech Min Sci* 128:104250
- Yang SQ, Jiang Y (2010) Triaxial mechanical creep behavior of sandstone. *Min Sci Techno* 20(3):339–349
- Yang XR, Jiang AN (2022) An improved nonlinear creep damage model of slates considering freeze–thaw damage and bedding damage. *B Eng Geol Environ* 81(6):240
- Yang SQ, Jing HW, Cheng L (2014) Influences of pore pressure on short-term and creep mechanical behavior of red sandstone. *Eng Geol* 179:10–23
- Yang SQ, Tang JZ, Wang SS, Yang DS, Zheng WT (2022) An experimental and modeling investigation on creep mechanical behavior of granite under triaxial cyclic loading and unloading. *Rock Mech Rock Eng* 55(9):5577–5597
- Yu CY, Tang SB, Tang CA, Duan D, Zhang YJ, Liang ZZ, Ma K, Ma TH (2019) The effect of water on the creep behavior of red sandstone. *Eng Geol* 253:64–74
- Yu MY, Liu BG, Liu KY, Sun JL, Deng TB, Wang Q (2023) Creep behavior of carbonaceous mudstone under triaxial hydraulic coupling condition and constitutive modelling. *Int J Rock Mech Min Sci* 164:105357
- Zhang T, Xu WY, Wang HL, Wang RB, Shi AC (2022) Experimental investigations on short-term and creep anisotropic mechanical behavior of artificial columnar jointed rock masses. *Rock Mech Rock Eng* 55(9):5393–5413
- Zhang C, Bai QS, Han PH (2023) A review of water rock interaction in underground coal mining: problems and analysis. *B Eng Geol Environ* 82(5):157
- Zhao K, Yang DX, Zeng P, Gong C, Wang XI, Zhong W (2021) Accelerating creep stage of red sandstone expressed and quantitatively identified based on acoustic emission information. *Rock Mech Rock Eng* 54:4867–4888
- Zhou ZL, Cai X, Ma D, Du XM, Chen L, Wang HQ, Zang HZ (2018) Water saturation effects on dynamic fracture behavior of sandstone. *Int J Rock Mech Min Sci* 114:46–61
- Zhou XP, Pan XK, Cheng H (2021) The nonlinear creep behaviors of sandstone under the different confining pressures based on NMR technology. *Rock Mech Rock Eng* 54(9):4889–4904
- Zhu J, Deng JH, Chen F, Ma YJ, Yao YF (2021) Water-Weakening effects on the strength of hard rocks at different loading rates: an experimental study. *Rock Mech Rock Eng* 54(8):4347–4353

**Publisher's Note** Springer Nature remains neutral with regard to jurisdictional claims in published maps and institutional affiliations.

Springer Nature or its licensor (e.g. a society or other partner) holds exclusive rights to this article under a publishing agreement with the author(s) or other rightsholder(s); author self-archiving of the accepted manuscript version of this article is solely governed by the terms of such publishing agreement and applicable law.